Multi-User Scheduling and Channel Characteristics for Water-to-Air Unmanned Vehicular Visible Light Communication

Tianjian Wei, Tianrui Lin, Nuo Huang, Chunfang Fu, Xinhui Liu, Liang Su, Li Tang, Qingqing Hu, and Chen Gong, *Senior Member, IEEE*

***Abstract*—In this paper, assuming that several underwater unmanned vehicles transmit data to one unmanned aerial vehicle above the water surface, we consider a multi-user water-to-air visible light communication system under wavy water conditions. Through Monte Carlo simulation and experiments, we extract link gains and analyze their statistic characteristics under different angles between the user line and the wave direction. Then, we propose two categories of scheduling schemes, namely scheduling schemes with and without interference among users, which are implemented under fixed-rate mode and delay-based allocated-rate mode, respectively. Moreover, we analyze the average system throughput and fairness of each scheduling scheme under different rate modes. The results show that simultaneous transmission schemes perform better in fixed-rate mode while orthogonal transmission schemes have higher throughput and are fairer in allocated-rate mode.**

***Index Terms*—Wavy water surface, multi-user scheduling, visible light communication, water-to-air communication.**

I. Introduction

With the increasing exploration of the ocean by human beings, underwater wireless communication has drawn great interest from both academic and industrial fields [1], [2], [3], [4]. One method is to place relay nodes on the water surface, but it leads to high equipment complexity and limited system scalability. For efficient data acquisition from the ocean, it is essential to establish a water-to-air (W2A) communication link across the water surface directly [5], [6], [7].

Radio frequency (RF) wave, acoustic wave and optical wave are three typical wireless carriers for transmission in the air and water. RF wave can travel a long distance (up to tens of kilometers) and achieve a high data rate (up to hundreds of Mbps) in the air, but it can propagate only a few meters in the water due to the high absorption and attenuation [8]. Acoustic wave is currently the primary scheme for underwater communication with long transmission distance (up to tens of kilometers) [9]. However, large delay, low data rate and severe reflection at the water surface hinder the application of acoustic wave in W2A communication. Considering the fact that neither RF wave nor acoustic wave is a good choice for communication across the water surface separately, a combination of them was proposed in [10] and [11], yielding the translational acoustic-RF communication (TARF). Acoustic waves propagate as pressure waves, creating tiny disturbances on water surface. An airborne radar can monitor and decode these disturbances for information recovery. Work [12] observed water surface amplitude characteristics of TARF system and adopt depth-corresponding signal-to-noise ratio as a performance metric. However, such system can only operate under a shallow depth (up to 60 cm) and a low data rate (up to 400 bps) at the expense of high system complexity.

Visible light communication (VLC) is a promising choice for communication across the water due to long transmission distance and high data rate. It has been demonstrated that water shows an acceptable light attenuation in the blue-green window (from 450 nm to 550 nm), which ensures adequate underwater link range [13]. Compared with RF and acoustic waves, VLC can provide high transmission rate (up to the order of Gbps) at relatively low power budget in both air and water [14].

Over the past year, extensive researches have been carried out on W2A-VLC. For W2A-VLC link, wavy water surface will lead to random spatial modulation on the light. Work [15] established a W2A link to extract the channel impulse response under different water surface conditions, whose statistics are fitted by typical probability distributions. In [16], the link gain and delay of W2A-VLC channel were evaluated through Monte Carlo simulation to exhibit the impact of ocean current when transmitter and receiver are not aligned. In [17], the characteristics of coverage and link gain for W2A-VLC were demonstrated and proved through experimental results. To improve the stability of W2A-VLC system, work [18] adopted two encoding schemes and analyzed their performance in dynamic environment. Work [19] investigated the influence of water waves on light spot and adopted multiple-input multiple-output

Manuscript received 4 February 2024; revised 7 June 2024; accepted 15 July 2024. Date of publication 29 July 2024; date of current version 19 December 2024. This work was supported in part by the National Natural Science Foundation of China under Grant 62171428 and Grant 62101526, and in part by the Fundamental Research Funds for the Central Universities under Grant KY2100000163. The review of this article was coordinated by Prof. Hayssam Dahrouj. *(Corresponding authors: Nuo Huang; Chen Gong.)*

Tianjian Wei, Tianrui Lin, Nuo Huang, Chunfang Fu, Qingqing Hu, and Chen Gong are with the CAS Key Laboratory of Wireless-Optical Communications, School of Information Science and Technology, University of Science and Technology of China, Hefei 230027, China (e-mail: weitj@mail.ustc.edu.cn; trlin@mail.ustc.edu.cn; huangnuo@ustc.edu.cn; fcf123@mail.ustc.edu.cn; ruixihu@mail.ustc.edu.cn; cgong821@ustc.edu.cn).

Xinhui Liu, Liang Su, and Li Tang are with the China Ship Scientific Research Center, Wuxi 214082, China (e-mail: liuxinhui@cssrc.com.cn; su.liangsu@163.com; tangli2012@pku.edu.cn).

Digital Object Identifier 10.1109/TVT.2024.3434967

structure to increase the achievable rate. Transmission rate was improved to 1.25 Gb/s in [20] via beam tracking and achieved 2.2 Gb/s in [21] via transmitter-side low-complexity digital signal processing. In [22], receiver-side photon distribution in laser channel model was investigated under different water surface conditions. However, there are few studies on the characteristics of multi-user W2A-VLC channel and find a suitable scheduling scheme for it. In work [23], multiple light sources were employed to increase the light intensity and coverage, but the channel characteristics were not mentioned. Work [24] combined acoustic and optical waves to investigate the performance of multi-user W2A relaying system. However, the performance was not validated via experiments, and the relaying system often incurs higher costs.

To find a balance between system performance (throughput or reliability) and user-level fairness is a significant problem in multi-user wireless communication system [25], [26], [27]. Adopting round-robin scheduling and opportunistic scheduling (greedy to the largest channel states among users) can achieve absolute fairness and performance. Work [28], [29] provided fair transmission time allocation for each user while a certain trade-off between performance and fairness was achieved in [30], [31] via adopting proportional fairness, based on relative channel strength of users. Work [32] concluded fairness measures and a model of joint optimization to achieve fairness.

In this paper, assuming that several underwater unmanned vehicles transmit data to one unmanned aerial vehicle above the water surface, we consider a multi-user W2A-VLC system through wavy water surface. We adopt light emitting diodes (LED) transmitters and avalanche photodiode (APD) receiver to extract W2A-VLC channel link gains via Monte Carlo simulation and experiments. Then, we analyze the statistical characteristics of link gains under different angles between the wave direction and the user line. Besides, we also conduct experiments for the anchored transmitters in the water current to simulate the shaking of underwater unmanned vehicle (UUV) under current waves. We adopt several scheduling schemes for this system and divide them into two categories according to interference situation among users. To approximate the real system, we take delay into account, which consists of transmission delay and processing delay. Then, scheduling schemes are utilized in two modes: fixed-rate mode and delay-based allocated-rate mode. Moreover, we adopt average system throughput and fairness as performance metrics of each scheduling scheme under different rate modes. It is observed that schemes with interference provide higher throughput and fairer performance to each user in fixed-rate mode. However, schemes without interference perform better in allocated-rate mode, in which round-robin is the fairest scheme.

The main contributions are summarized as follows.

- Under the assumption of user independence and static channel, we present a multi-user W2A-VLC system model and adopt intensity-modulation/direct-detection (IM/DD) for data transmission. The achievable rate for each user is given under a truncated Gaussian (TG) input distribution.
- We adopt Monte-Carlo simulations and experiments in different scenarios to extract the link gain of multi-user W2A-VLC channel with three LED transmitters and one APD receiver. According to simulation and experimental results, we obtain characteristics of multi-user W2A-VLC channel under different positions and wave scales.
- We demonstrate the impacts of delay and waving water surface on system performance via analyzing the throughputs and minimum rates of different scheduling schemes. Moreover, we compare different schemes and choose the optimal one in different relative positions and rate modes.

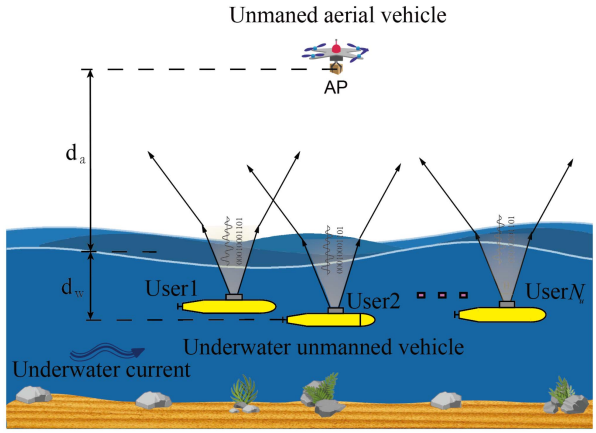

Fig. 1. Illustration of the considered W2A-VLC system.

The rest of this paper is organized as follows. Section II introduces the multi-user W2A-VLC system model. In Section III, scheduling schemes and performance metrics are introduced. In Section IV, the simulation and laboratory experiment results are presented to provide preliminary W2A-VLC channel characteristics. Then, in Section V, data collected from a more realistic deep-wave-pool scenario is adopted to show the influence of fluctuating water surface and relative positions. Finally, Section VI concludes this paper.

II. System Descriptions

A. Multi-User W2A-VLC Scenario

Fig. 1 illustrates a multi-user W2A-VLC system where N_u users under the water send data to one access point (AP) in the air. Each user is equipped with one green/blue LED transmitter at depth d_w under water surface, while the AP is equipped with one APD receiver at height d_a above water surface. Each LED with beam angle θ transmits the optical signal to the APD. The light first propagates in the water, then penetrates into the air after being refracted at the water surface, and finally is detected by the APD for further processing.

In contrast to VLC system in the atmosphere, the most significant feature in W2A-VLC is the dynamic signal intensity caused by water surface fluctuation. In this work, we adopt the AP to control users and investigate the performance of different access schemes.

B. System Model and Channel Capacity

Let h_i $(i = 1, 2, \ldots, N_u)$ denote the compound channel gain including both underwater and ground-above components from

user i to the AP, which can be estimated from pilot signals. The channel estimate is carried out in the electrical domain and sent back to the transmitter for further processing. Assume that in each transmission period, h_i remains constant and will change to an independent state in the next period [19]. Without loss of generality, assume $h_1 \geq h_2 \geq \cdots \geq h_{N_u}$. The received signal in transmission period l is given by

$$y[l] = \sum_{i=1}^{N_u} h_i x_i[l] + z[l], \quad l = 1, 2, \ldots, L, \tag{1}$$

where $x_i[l]$ denotes the transmitted signal of user i, $z[l]$ denotes the zero-mean Gaussian noise with variance σ^2, and L denotes the number of transmission periods. We adopt IM/DD in W2A-VLC system, where the information is modulated on the light intensity and the receiver recovers the data based on the received signal intensity. Under the non-negativity, identical peak and average power constraints, we have

$$x_i \geq 0,\ x_i \leq A,\ \mathbb{E}[x_i] \leq \varepsilon, \quad \forall i = 1, \ldots, N_u. \tag{2}$$

Denote the user set as $\mathcal{U} \triangleq \{1, 2, \ldots, N_u\}$. Let $\mathcal{E}$ and $\mathcal{F}$ respectively denote the signal set and interference set, which are two disjoint subsets of $\mathcal{U}$ and satisfy $\mathcal{E} \cup F = U$. Considering the time-varying interference from other users in SIC-based scheduling schemes, we define the transmitter-side peak-to-noise ratio (PNR) as A/σ.

To approximate the channel capacity, we adopt a TG input distribution [33] with mean $\hat{\mu}$ and variance $\hat{\nu}^2$, which can be expressed as

$$\theta^A_{\mu,\nu}(x) = \begin{cases} \lambda g_{\mu,\nu}(x), & x \in [0, A] \\ 0, & \text{otherwise} \end{cases}, \tag{3}$$

where $g_{\mu,\nu}(x)$ is the Gaussian distribution with mean μ and variance ν^2; $\lambda = (G_{\mu,\nu}(A) - G_{\mu,\nu}(0))^{-1}$ and $G_{\mu,\nu}$ is the corresponding cumulative Gaussian distribution. Under the constraints in (2), the mean $\hat{\mu}$ and variance $\hat{\nu}^2$ are given by

$$\begin{aligned} \hat{\mu} &= \nu^2[\theta^A_{\mu,\nu}(0) - \theta^A_{\mu,\nu}(A)] + \mu, \\ \hat{\nu}^2 &= \nu^2[1 - A\theta^A_{\mu,\nu}(A) - \hat{\mu}(\theta^A_{\mu,\nu}(0) - \theta^A_{\mu,\nu}(A))]. \end{aligned} \tag{4}$$

Assume that the N_u users transmit information at rates $R_1, \ldots, R_{N_u}$. From the achievable rates for multi-user scenario, we have

$$\sum_{i \in \mathcal{E}} R_i \leq I(\mathcal{E}; Y|\mathcal{F}), \tag{5}$$

where

$$\begin{aligned} I(\mathcal{E}; Y|\mathcal{F}) &= h(Y|\mathcal{F}) - h(Y|\mathcal{E}, \mathcal{F}) \\ &= h\left(\sum_{i \in \mathcal{E}} X_i + Z\right) - h(Z). \end{aligned} \tag{6}$$

Assuming that all users operate with the same three-tuple parameter (μ, ν, A), the following region for user set $\mathcal{U}$ can be achieved [34]

$$\begin{aligned} \mathcal{C}_{\mathcal{U}} = \Bigg\{ \boldsymbol{R} : \sum_{i=1}^{|\mathcal{E}|} R_{\mathcal{E}[i]} \leq -\sum_{i=1}^{|\mathcal{E}|} \phi_{\mathcal{E}[i]} + \frac{1}{2} \sum_{i=1}^{|\mathcal{E}|} \Bigg[\log \nu^2 \\ - \log \left(\hat{\nu}^2 - \frac{h^2_{\mathcal{E}[i]} \hat{\nu}^4}{\sum_{p=i}^{|\mathcal{E}|} h^2_{\mathcal{E}[p]} \hat{\nu}^2 + \sigma^2} \right) \Bigg], \forall \mathcal{E} \subseteq \mathcal{U} \Bigg\}, \end{aligned} \tag{7}$$

where $\phi = \log \lambda + \frac{1}{2}((A - \mu)\theta^A_{\mu,\nu}(A) + \mu\theta^A_{\mu,\nu}(0))$; $\mathcal{E}[i]$ denotes the i-th element of set $\mathcal{E}$ and $|\mathcal{E}|$ denotes the number of elements in set $\mathcal{E}$. The rate region given by (4) is a N_u-dimensional polyhedron with $N_u!$ corner points [35], which can be achieved via SIC.

We adopt two rate modes in multi-user W2A-VLC system: allocated-rate mode and fixed-rate mode. For rate allocation, the AP extracts link gain of user i and chooses an appropriate rate in a transmission period. In real system, the delay should be taken into account, including transmission delay and processing delay. Thus, after a certain delay τ, $R_i[l - \tau]$ can be allocated to user i in transmission period l. For another mode, each user obtains a fixed rate $R_i[l - \tau] = R_i$ before transmission.

Remark 1: Different from radio-frequency communication in terrestrial networks, there is no closed-form expression for exact capacity results of VLC. Thus, we compute the achievable rate based on the lower bound.

III. Scheduling Scheme and Performance Metrics

In this section, we first propose round-robin, competition and SIC-based scheduling schemes for multi-user W2A-VLC system. Then, we analyze the throughput and minimum rate of the proposed schemes as performance metrics.

A. Scheduling Without Interference Among Users

We first consider transmission of each users without interference from other users. For user i, we adopt a delay-based indicator function to indicate the outage during transmission period l [36]:

$$I_{\tau,i}[l] = \begin{cases} 1, R_i[l - \tau] \leq C_i[l] \\ 0, R_i[l - \tau] > C_i[l] \end{cases}. \tag{8}$$

This function means that the outage occurs when $R_i[l - \tau] > C_i[l]$ in transmission period l. $C_i[l]$ is the lower bound on channel capacity and can be calculated as (7).

1) Round-Robin Scheduling: In round-robin scheduling, each user occupies an equal amount of transmission time, and the AP allocates time slots to each user in turn. Define the average system throughput to be the total bits per channel use that are successfully delivered to the AP, i.e.,

$$\rho = \frac{1}{N_u} \sum_{i=1}^{N_u} \sum_{l=1+\tau}^{L} \frac{I_{\tau,i}[l] R_i[l - \tau]}{L - \tau}. \tag{9}$$

2) Delay-Based Competition Scheduling: In the competition scheduling, the user with the largest link gain is accessed, i.e., user 1 under the assumption $h_1 \geq h_2 \geq \cdots \geq h_{N_u}$. Then, the

average system throughput during L transmission periods can be expressed as

$$\rho = \sum_{l=1+\tau}^{L} \frac{I_{\tau,\tilde{i}}[l]\tilde{R}_i[l-\tau]}{L-\tau}, \tag{10}$$

where $\tilde{i} = \arg\max\{R_1[l-\tau], R_2[l-\tau], \ldots, R_{N_u}[l-\tau]\}$ and $\tilde{R}_i[l-\tau] = \max\{R_1[l-\tau], R_2[l-\tau], \ldots, R_{N_u}[l-\tau]\}$.

B. Scheduling With Interference Among Users

In round-robin and competition scheduling, the opportunity of access can be allocated to only one user in a single transmission period. Now, considering that all users access to the channel in each transmission period, we adopt SIC for user decoding and successive group decoding (SGD) as an optimization.

In SIC, the main idea is to select a decoding order and decode each user individually via treating the remaining users as interference [37]. It has been proven that the optimal decoding order is the descending trend of link gain [38]. Thus, in decoding stage of user i, the received signal to be processed by AP can be expressed as

$$y[l] = h_i x_i[l] + \left(\sum_{j=i+1}^{N_u} h_j x_j[l] + z[l] \right), \quad l = 1, 2, \ldots, L, \tag{11}$$

where $\sum_{j=i+1}^{N_u} h_j x_j[l] + z[l]$ is treated as the additive noise. Then, the achievable rate can be derived as

$$R_i = -\phi + \frac{1}{2}\left[\log \nu^2 - \log\left(\hat{\nu}^2 - \frac{h_i^2 \hat{\nu}^4}{\sum_{j \geq i} h_j^2 \hat{\nu}^2 + \sigma^2}\right)\right]. \tag{12}$$

SGD is an extension of the SIC which decode a group of users instead of one in each stage. After removing the decoded users, one group of users are jointly decoded via maximum likelihood detection while treating the remaining users as interference. Therefore, multi-complexity decoder can be adopted during decoding, i.e., successive decoder among groups and maximum-likelihood decoder within single group [39]. Based on the same optimality criteria, the ordered partition of users is denoted by $\mathcal{G} = \{\mathcal{G}_1, \ldots, \mathcal{G}_p\}$. Let $\mathcal{C}_{\mathcal{G}_k}$ and $\boldsymbol{R}_{\mathcal{G}_k}$ represent the achievable rate region and rate vector for users in group K. Similar to (11), the received signal in decoding stage of group $\mathcal{G}_k$ can be expressed as

$$y[l] = \sum_{i \in \mathcal{G}_k} h_i x_i[l] + \left(\sum_{j \in \mathcal{U} \setminus \cup_{m=1}^{k} \mathcal{G}_m} h_j x_j[l] + z[l] \right), \tag{13}$$

where $l = 1, 2, \ldots, L$. Then, according to (7), we have

$$\mathcal{C}_{\mathcal{G}_k} = \left\{ \boldsymbol{R} : \sum_{i=1}^{|\mathcal{D}|} R_{\mathcal{D}[i]} \leq -\sum_{i=1}^{|\mathcal{D}|} \phi_{\mathcal{D}[i]} + \frac{1}{2} \sum_{i=1}^{|\mathcal{D}|} \left[\log \nu^2 - \log \left(\hat{\nu}^2 - \frac{h_{\mathcal{D}[i]}^2 \hat{\nu}^4}{\sum_{p=i}^{|\mathcal{D}|} h_{\mathcal{D}[p]}^2 \hat{\nu}^2 + \sum_{j \in \mathcal{U} \setminus \cup_{m=1}^{k} \mathcal{G}_m} h_j^2 \hat{\nu}^2 + \sigma^2} \right) \right], \forall \mathcal{D} \subseteq \mathcal{G}_k \right\}. \tag{14}$$

Algorithm 1: Decoding Order and Partitioning for Fixed Rates.

1: Initialize $\mathcal{E} \triangleq \{1, \ldots, N_u\}$, $\mathcal{G} = \emptyset$ and fixed-rate vector $\boldsymbol{R}$.
2: $\delta = \max_{\mathcal{G}_k \neq \emptyset, \mathcal{G}_k \subset \mathcal{E}} \Theta_k(\boldsymbol{h}_{\mathcal{G}_k}, \mathcal{G}_k, \mathcal{E} \setminus \cup_{m=1}^{k} \mathcal{G}_m, \boldsymbol{R}_{\mathcal{G}_k})$.
3: $\mathcal{G}_{opt} = \underset{\mathcal{G}_k \neq \emptyset, \mathcal{G}_k \subset \mathcal{E}}{\arg\max}\ \Theta_k(\boldsymbol{h}_{\mathcal{G}_k}, \mathcal{G}_k, \mathcal{E} \setminus \cup_{m=1}^{k} \mathcal{G}_m, \boldsymbol{R}_{\mathcal{G}_k})$.
4: **if** $\delta < 0$ **then**
5: Declare an outage and Stop.
6: **else**
7: Update $\mathcal{E} \leftarrow \mathcal{E} \setminus \mathcal{G}_{opt}$ and $\mathcal{G} \leftarrow \{\mathcal{G}, \mathcal{G}_{opt}\}$.
8: **if** $\mathcal{E} = \emptyset$ **then**
9: Output $\mathcal{G}$ and Stop.
10: **else**
11: Go to Step 2.
12: **end if**
13: **end if**

Note that SIC is a special case of SGD with $|\mathcal{G}_k| = 1$, for $\forall 1 \leq k \leq p$.

1) Fixed Rate for Each User: Assume that user i is allocated with fixed rate $R_i[l] = R_i$ before transmission, for $\forall i \in \mathcal{U}$, $l = 1, 2, \ldots, L$. The gap between the actual rate and the boundary of achievable rate region is given by [40]

$$\Delta(h, \mathcal{E}, \mathcal{F}, \boldsymbol{R}) = -\sum_{i=1}^{|\mathcal{E}|} \phi_{\mathcal{E}[i]} + \frac{1}{2} \sum_{i=1}^{|\mathcal{E}|} \left[\log \nu^2 - \log \left(\hat{\nu}^2 - \frac{h_{\mathcal{E}[i]}^2 \hat{\nu}^4}{\sum_{p=i}^{|\mathcal{E}|} h_{\mathcal{E}[p]}^2 \hat{\nu}^2 + \sum_{j \in \mathcal{F}} h_j^2 \hat{\nu}^2 + \sigma^2} \right) \right] - \sum_{i=1}^{|\mathcal{E}|} R_i. \tag{15}$$

Define

$$\Theta_k(\boldsymbol{h}_{\mathcal{G}_k}, \mathcal{G}_k, \mathcal{U} \setminus \cup_{m=1}^{k} \mathcal{G}_m, \boldsymbol{R}_{\mathcal{G}_k}) = \min_{\mathcal{D} \subseteq \mathcal{G}_k, \mathcal{D} \neq \emptyset} \left\{ \Delta(\boldsymbol{h}_{\mathcal{G}_k}, \mathcal{D}, \mathcal{U} \setminus \cup_{m=1}^{k} \mathcal{G}_m, \boldsymbol{R}_{\mathcal{D}}) \right\}. \tag{16}$$

For each group, the allocated fixed-rates can be achieved if $\Theta_k(\boldsymbol{h}_{\mathcal{G}_k}, \mathcal{G}_k, \mathcal{U} \setminus \cup_{m=1}^{k} \mathcal{G}_m, \boldsymbol{R}_{\mathcal{G}_k}) \geq 0$, and outage occurs if and only if $\min_{1 \leq k \leq p} \Theta_k < 0$.

Algorithm 1 outlines the procedure for optimal group partition and decoding order in fixed-rate mode. In line 2, function Θ_k selects the group with the smallest gap between given rates and capacity lower bound, with the additional function $\max$ to minimizes the outage events.

2) Rate Allocation for Each User: Beyond fixed-rate mode, we address channel-dependent rate allocation for individual users. The AP calculates $R_i[l]$ through h_i extracted from the pilot signal in transmission period l and allocates it to user i.

Algorithm 2 presents the process of obtaining the optimal group partition, decoding order and throughput-maximized rate

Algorithm 2: Decoding Order and Partitioning for Rate Allocation.

1: Initialize $\mathcal{E} \triangleq \{1, \ldots, N_u\}$, $\mathcal{F} = \emptyset$, $\mathcal{G}_k = \emptyset$ and $k = 1$, set $\boldsymbol{G}$ and $\boldsymbol{R}$ to be all-zero vectors.
2: **repeat**
3: $R_{\mathcal{G}_k} = \alpha \cdot \min_{\mathcal{D}\neq\emptyset, \mathcal{D}\subset\mathcal{E}} \Delta(\boldsymbol{h}_\mathcal{D}, \mathcal{D}, \mathcal{F}, 0)/|\mathcal{D}|$.
4: $\mathcal{G}_k = \arg\min_{\mathcal{D}\neq\emptyset, \mathcal{D}\subset\mathcal{E}} \Delta(\boldsymbol{h}_\mathcal{D}, \mathcal{D}, \mathcal{F}, 0)$.
5: $\mathcal{E} = \mathcal{E} \setminus \mathcal{G}_k$, $\mathcal{F} = \mathcal{F} \cup \mathcal{G}_k$.
6: $k = k + 1$.
7: **until** $\mathcal{E} = \emptyset$
8: $\boldsymbol{G}[i] \leftarrow \mathcal{G}_{k-i}$, $\boldsymbol{R}[i] = R_{\mathcal{G}_{k-i}}$, $i \in [1, k-1]$.
9: Output $\boldsymbol{G}$, $\boldsymbol{R}$.

allocation. When $R_i = 0$, $\Delta(h, \mathcal{E}, \mathcal{F}, \boldsymbol{R})$ represents the sum rate for a user group. Thus, we adopt (15) to allocate the same rate to users within a group with constant α balancing outage probabilities and rates, particularly when considering delays. Use $\boldsymbol{G}$ to record the optimal order.

Note that the main complexity of Algorithm 1 lies in solving the optimization problem in line 2. We first adopt a greedy algorithm for computation of (16) with complexity $\mathcal{O}(|\mathcal{G}_k|)$. Then, we nest a greedy algorithm with complexity $\mathcal{O}(|\mathcal{E}|)$ to choose a subset of signal set $\mathcal{E}$ with maximum Θ_k. Steps 4-12 determine the decoding order in at most $|\mathcal{E}|$ times. Thus, the complexity of Algorithm 1 is at most $\mathcal{O}(|\mathcal{E}|^{|\mathcal{G}_k|+1})$. With rate allocation, we do not calculate the gap in Algorithm 2 and can adopt a typical dynamic programming algorithm with complexity at most $\mathcal{O}(|\mathcal{E}|^2)$.

Remark 2: Due to the wave current-induced fast fading [19], rate allocation scheduling schemes demonstrate higher throughput than round-robin and competition schemes only under short delay.

3) Throughput and Minimum Rate: Similar to the case with no interference, the average system throughput of SIC and SGD can be expressed as

$$\rho = \sum_{i=1}^{N_u} \sum_{l=1+\tau}^{L} \frac{I_{\tau,i}[l] R_i[l-\tau]}{L-\tau}, \tag{17}$$

where the achievable rate for each user in indicator function can be calculated via (12) and (14).

In addition, to illustrate the fairness of each scheme, we adopt the following minimum achievable rate as another performance metric

$$\min_{i\in\mathcal{U}} \left(\left(\frac{\sum_l I_{\tau,i}[l]}{L-\tau} \right) \cdot \min_l R_i[l-\tau] \right), \quad l \in \{1+\tau, 2+\tau, \ldots, L\}. \tag{18}$$

Minimum rate for fixed-rate mode is a special case of (18) with $\tau = 0$.

IV. Simulation and Laboratory Experiments

In this section, simulation and laboratory results are provided to extract the link gain of multi-user W2A-VLC channel. Fig. 2 provides a schematic diagram for two situations in simulation and experiments: the line connecting three LEDs vertical and parallel to wave direction, which are labeled as "vertical" and "parallel", respectively.

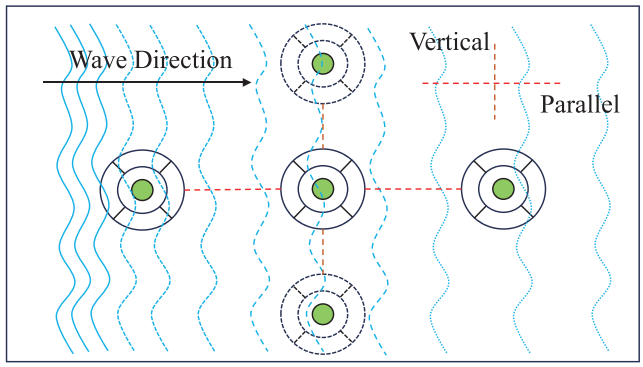

Fig. 2. Illustration for related positions of users and wave direction.

TABLE I
Parameters in Different Cases

	Direction	d_a(m)	Spacing(m)	d_w(m)
Simulation	Parallel	10	5	10
	Vertical	10	5	10
Laboratory	Parallel	1.9	0.4	0.2
	Vertical	1.9	0.3	0.2

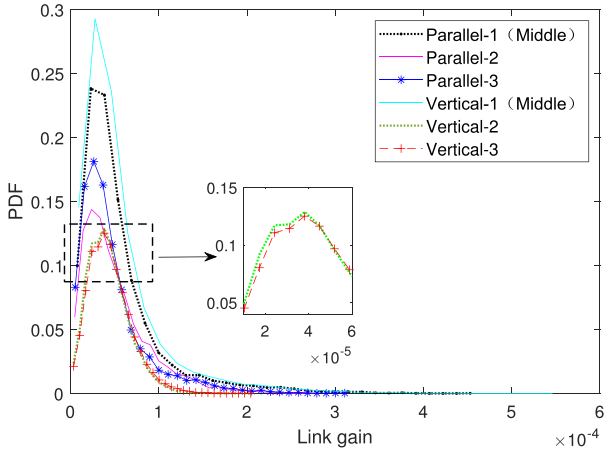

Fig. 3. PDF of link gain from simulation.

A. Simulation

We simulate the multi-user W2A-VLC link gain based on ray tracing. Each ray will undergo multiple refractions in the water and water surface before propagating in the atmosphere [16]. An AP above the water surface receives each ray and the link gain will be extracted via subsequent processing. Detailed parameters are shown in Table I.

The link gain variation under different relative positions is shown in Fig. 3. In case of parallel, the link gains from different nodes tend to be different; in case of vertical, the peaks tends to overlap with each other.

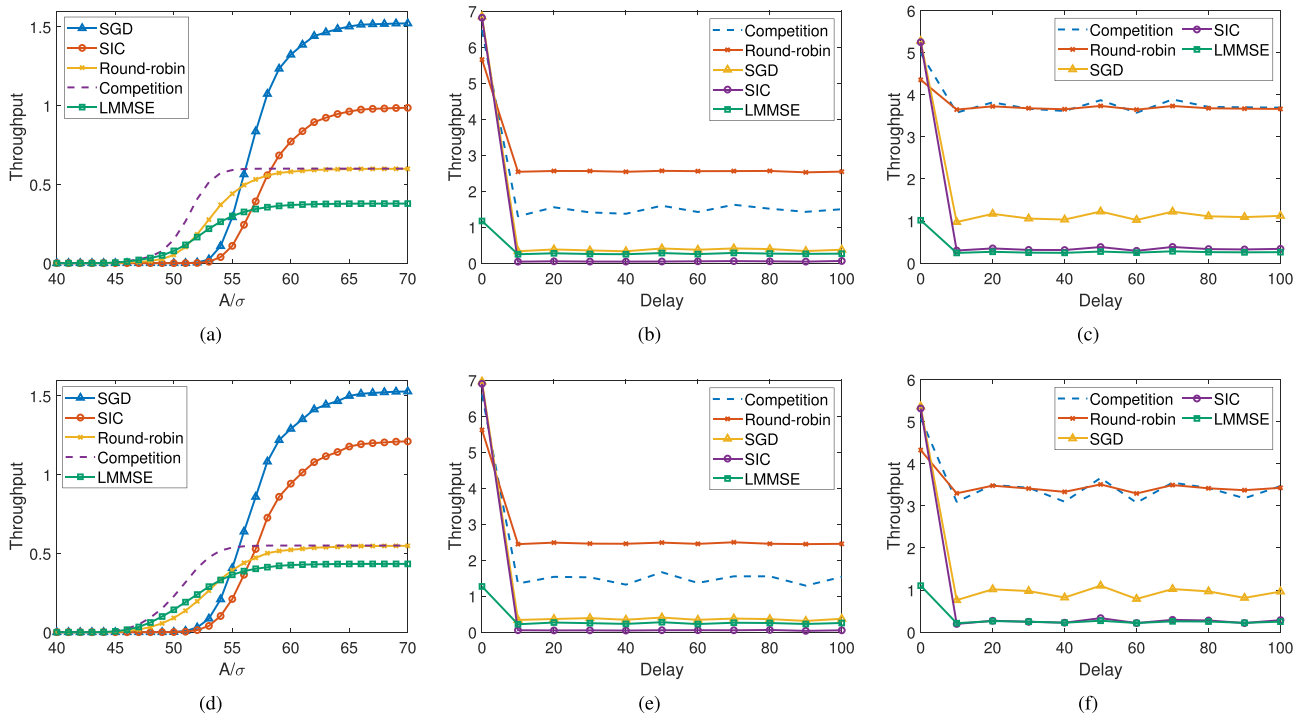

Fig. 4. Influence of related positions and rate modes on the throughput. (a) Vertical, fixed-rate. (b) Vertical, allocated-rate. (c) Vertical, optimal allocated-rate. (d) Parallel, fixed-rate. (e) Parallel, allocated-rate. (f) Parallel, optimal allocated-rate.

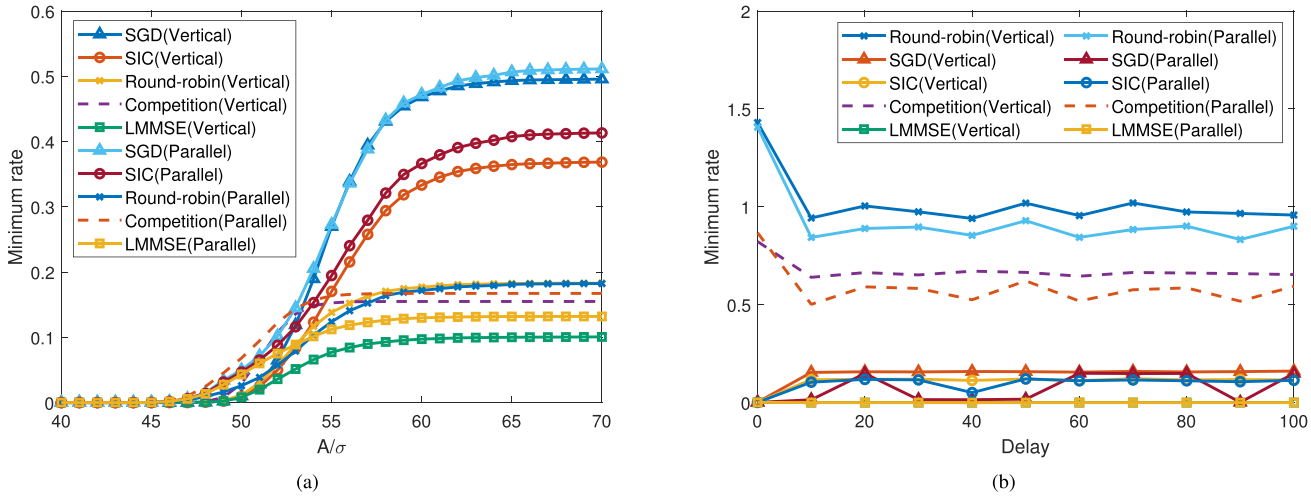

Fig. 5. Minimum rate for each strategies. (a) Fixed-rate. (b) Optimal allocated-rate.

We analyze link gain data through the aforementioned schemes, as shown in Fig. 4. Specifically, Fig. 4(a) and (d) show the throughput under different PNRs. It is seen that, in fixed-rate mode, SGD shows the minimum outage and largest throughput for A/σ higher than 50 dB. However, considering rate allocation and delay, the advantage of max-min allocation will disappear, as shown in Fig. 4(b) and (e). Due to better stability, round-robin and competition scheduling show higher throughput than SIC-based schemes.

In Algorithm 2, we first greedily allocate rate to each users, which will easily lead to outage with long delay and fluctuating channel. Thus, we multiplied allocated-rate by a coefficient changing in [0,1] to achieving a trade-off between rate and outage. An easy fixed-step cycle algorithm is added to Algorithm 2 to choose an optimal coefficient with the highest throughput. Comparing Fig. 4(b) and (c), Fig. 4(e) and (f), each scheme gains a significant improvement while round-robin and competition still shows the highest throughput. In addition, the gap between round-robin and competition is reduced after optimization because of lower outage probability in latter scheme.

Fig. 5 shows the fairness performance of each scheme. In fixed-rate case, as shown in Fig. 5(a), SGD shows the best

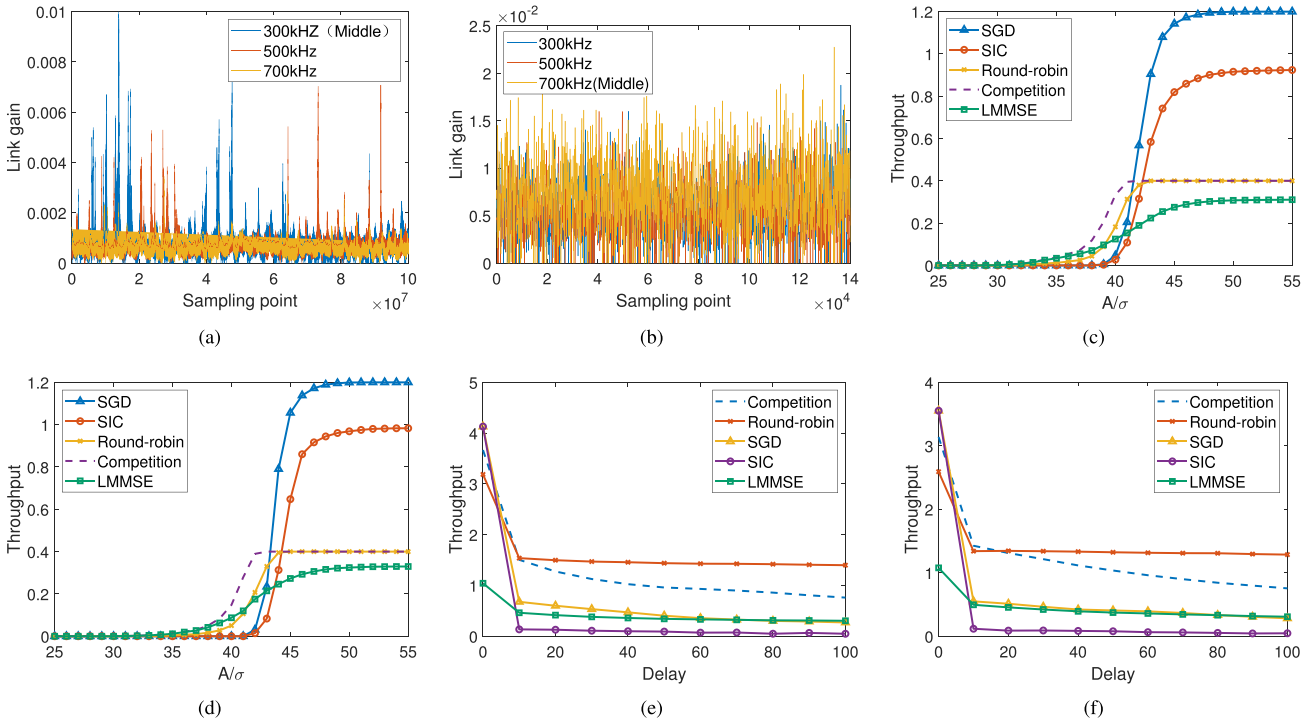

Fig. 6. Link gain variation and laboratory performance in different related positions and rate modes. (a) Link gain, regular wave. (b) Link gain, broken wave. (c) Throughput, vertical, fixed-rate. (d) Throughput, parallel, fixed-rate. (e) Throughput, vertical, allocated-rate. (f) Throughput, parallel, allocated-rate.

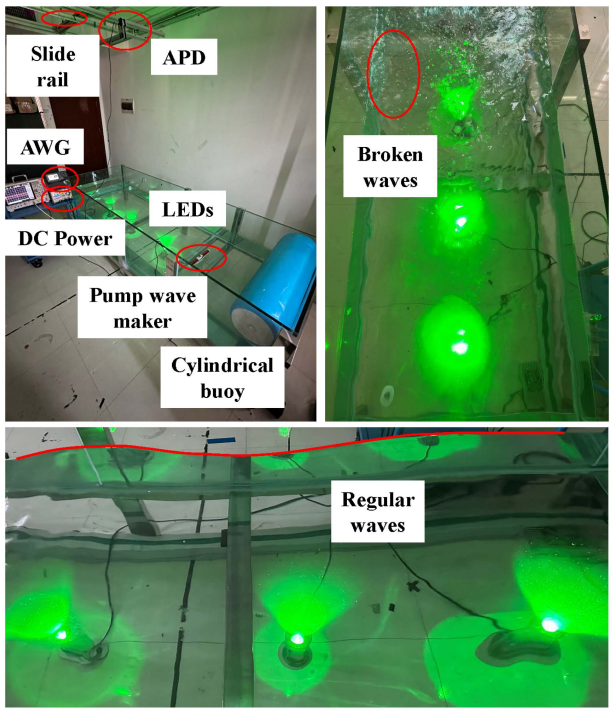

Fig. 7. Actual scenarios in the laboratory. (a) LEDs and APD. (b) Broken waves. (c) Regular waves.

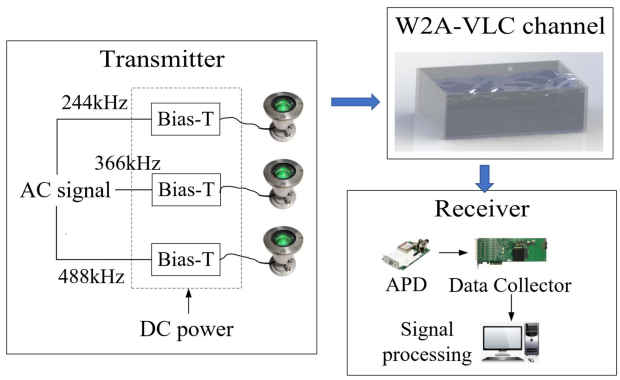

Fig. 8. Block diagram for the multi-user W2A-VLC system.

performance lower bound because of higher throughput when outage probability for each scheme is low. Meanwhile, taking delay into account, round-robin holds the fairest performance due to the similar access opportunities and no interference for each user.

B. Experiment in Laboratory Water Tank

We adopt three green LEDs (Cree XBDGRN, 520 nm ∼ 535 nm, 3-dB bandwidth: 5 MHz) sealed in separate underwater containers as transmitters. The LEDs are placed in the direction of vertical and parallel to waves, whose spacing is 0.3 m as shown in Fig. 7(a). We use three bias-tee circuits, which combines the DC bias (DC = 7 V) from a DC power supply (Rigol DP832 A) with sine signal generated by an arbitrary waveform generator (Rigol DG5252). In order to distinguish the three users, we assign different frequencies to them, which are 300 kHz, 500 kHz and 700 kHz. Via a lens, the light beam angle is concentrated to approximately 30°.

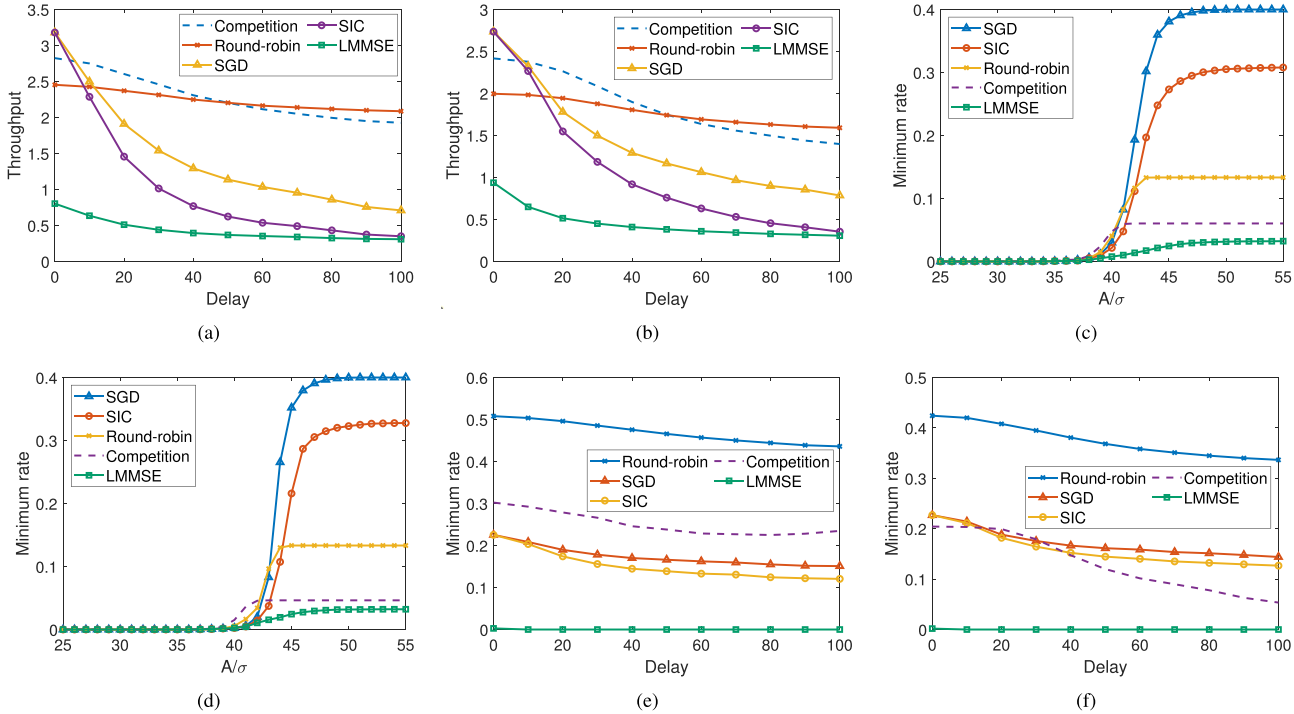

Fig. 9. Optimization for rate allocation and fairness for each strategy. (a) Throughput, vertical, optimal allocated-rate. (b) Throughput, parallel, optimal allocated-rate. (c) Minimum rate, vertical, fixed-rate. (d) Minimum rate, parallel, fixed-rate. (e) Minimum rate, vertical, optimal allocated-rate. (f) Minimum rate, parallel, optimal allocated-rate.

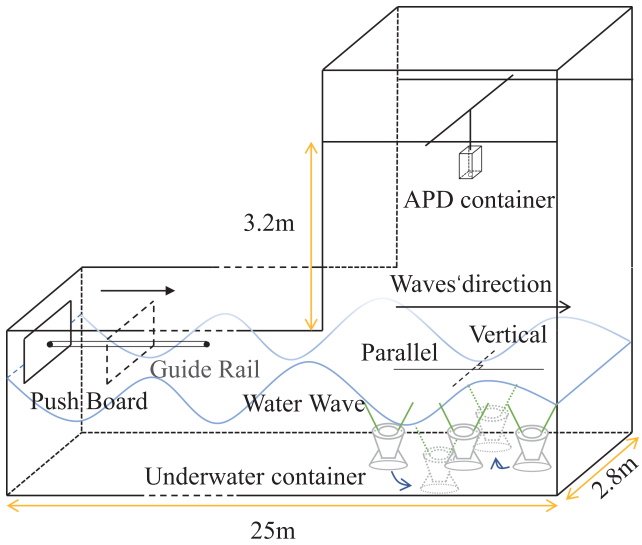

Fig. 10. Schematic diagram of deep wave pool.

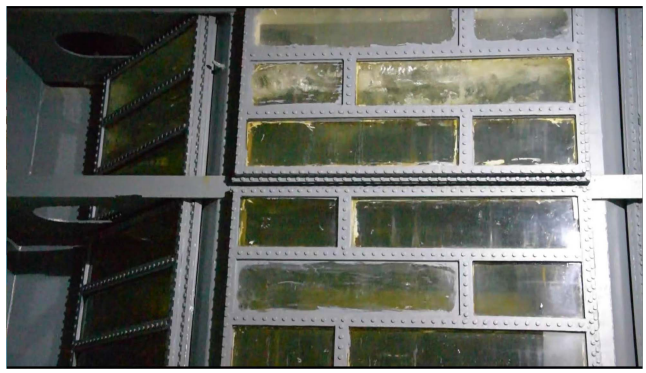

Fig. 11. Actual scenario of deep wave pool.

In the laboratory, we adopt different wave-making equipments to generate different types of waves. As shown in Fig. 7(b), we place a pump wave generator underwater on each side of the water tank. Fig. 7(c) shows a regular wave with a shape similar to a sine wave via pressing cylindrical buoy. Actually, due to limited length of water tank, standing waves will exist for a long time.

At height 1.9 m above the water surface, a DC-blocking APD (Hamamatsu C12702-11, bandwidth 50 kHz–40 MHz) with an amplification circuit is placed as the receiver. After propagating through the W2A link, the optical signal is received by the APD. A data collector (ART Technology PCIe8584, 100MSa/s) is adopted to sample the APD output signal for further processing, as shown in Fig. 8.

Fig. 6(a) and (b) show the experimental link gains in laboratory. It is seen that the wave model has a significant impact on the variation of link gain. Specifically, as shown in Fig. 6(a), the variation of link gain exhibits a similar periodicity because of regular wave; while under broken waves, the changes in link gain are more chaotic, as seen in Fig. 6(b).

Fig. 6(c)–(f) illustrate the throughput of different access schemes. As shown in Fig. 6(c) and (d), under fixed rate, SGD scheme shows the largest throughput due to simultaneous user

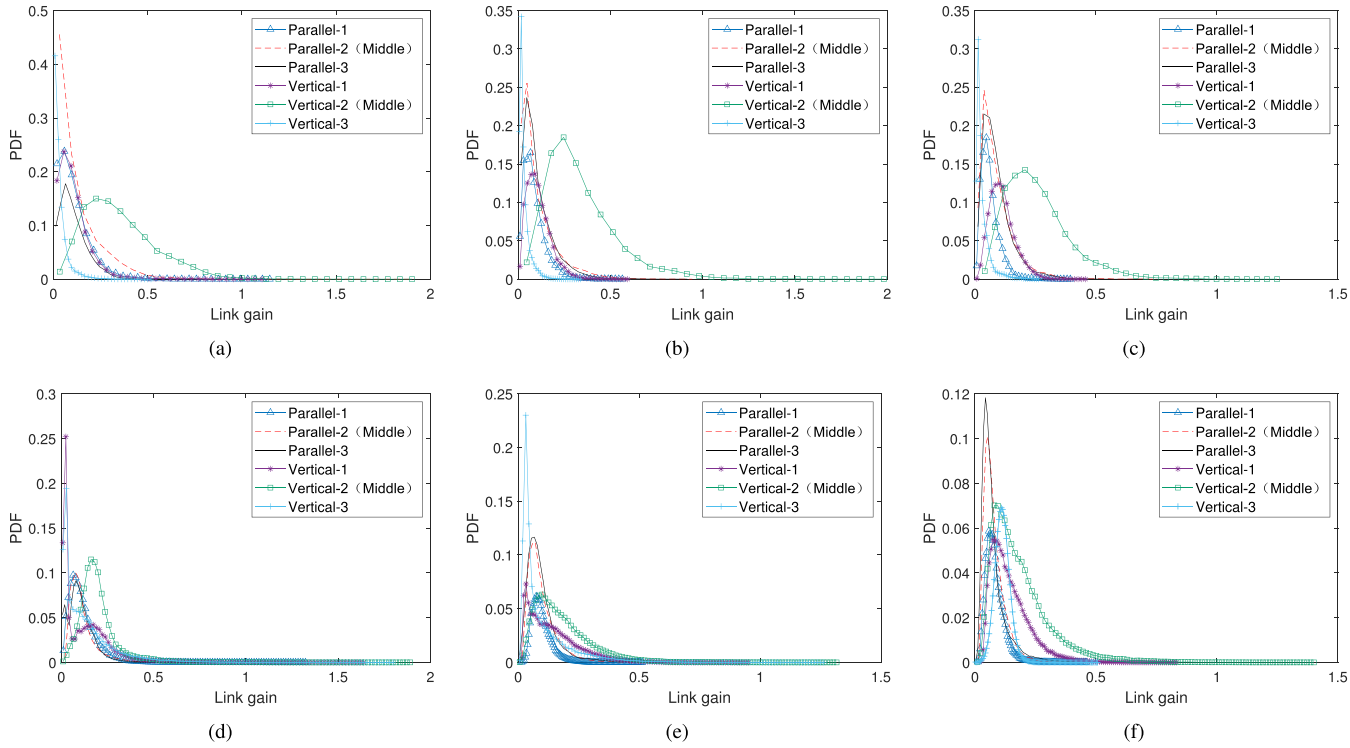

Fig. 12. The PDF of link gain in deep water pool. (a) Depth = 0.3 m, fixed container. (b) Depth = 0.5 m, fixed container. (c) Depth = 0.7 m fixed container. (d) Depth = 0.3 m, anchored container. (e) Depth = 0.5 m, anchored container. (f) Depth = 0.7 m anchored container.

access and optimal group decoding order. Then, in Fig. 6(e) and (f), SGD shows the highest throughput under small delay. However, for delay longer than 1 ms, the round-robin scheme shows the highest throughput due to independent user channel access.

For laboratory results, we adopt similar processing to optimize rate allocation, as shown in Fig. 9(a) and (b). When the delay is longer than 10 ms, round-robin and competition hold higher throughput because of no interference among users. When the delay is longer than about 50 ms, round-robin maintains the highest throughput. The reason is that the competing user access, which allocates all the resource to one user, will easily lead to outage in a fluctuation channel. For fairness, in Fig. 9(c) and (d), SGD shows the highest minimum rate under fixed rate mode. Meanwhile, round-robin shows the highest throughput under rate allocation.

V. Performance Analysis in Deep Wave Pool

We also conduct experiments in a deep wave pool with size 25 m long, 2.8 m wide and 6 m depth. A wave generator is adopted to generate regular wave, where the height and wavelength of waves can be controlled. Then, we remove the baffle inside the pool wall to create broken waves vertical to regular waves.

As shown in Fig. 10, the transmitters are concealed in waterproof containers fixed on a lift platform. The interval between each container can be up to 0.6 m and underwater depth changes from 0.3 m to 0.7 m with 0.2 m each step. Moreover, the containers are anchored to the platform via steel cables to simulate the shaking of UUVs under current waves.

An APD is suspended on an XY-slide 3.2 m above the water surface and can be easily moved above the intermediate node. The outputs from APD are sampled by a high-speed data collector, whose sampled data will be processed in an offline manner. At each depth, we collect data in 120 seconds. An actual scenario graph taken from outside can be seen in Fig. 11.

Due to the collision with waves from other directions, there will be many small broken waves superimposed on regular waves. In general, the waves in deep water pool consists of a mixture of large-scale regular waves and small-scale broken waves.

Fig. 12 shows the PDF of link gain in different LED positions. It can be seen that the waves in deep pools exhibit both large-scale regularity and small-scale fluctuation, which is consistent with the characteristics of mixed waves and is similar to those in Fig. 5(a) and (c). Due to larger user spacing and depth, the effect of location characteristics on link gain is more evident than those in Fig. 3. When the transmitters are anchored in the water current, the link gain distributions tend overlap more in both scenarios where the transmitters are vertical and parallel to the wave direction, due to the effect of shaking.

Specifically, in vertical situation, the middle user maintains great advantage to others from the perspective of link gain. For example, in the third row in Table II, the middle user achieves the largest mean channel gain also far greater than other users. Then, in Fig. 12(a), the middle user can achieve higher link gain because it has a longer trailing than the curve of other users. Compared with that in Fig. 3, the PDF curve of middle user in

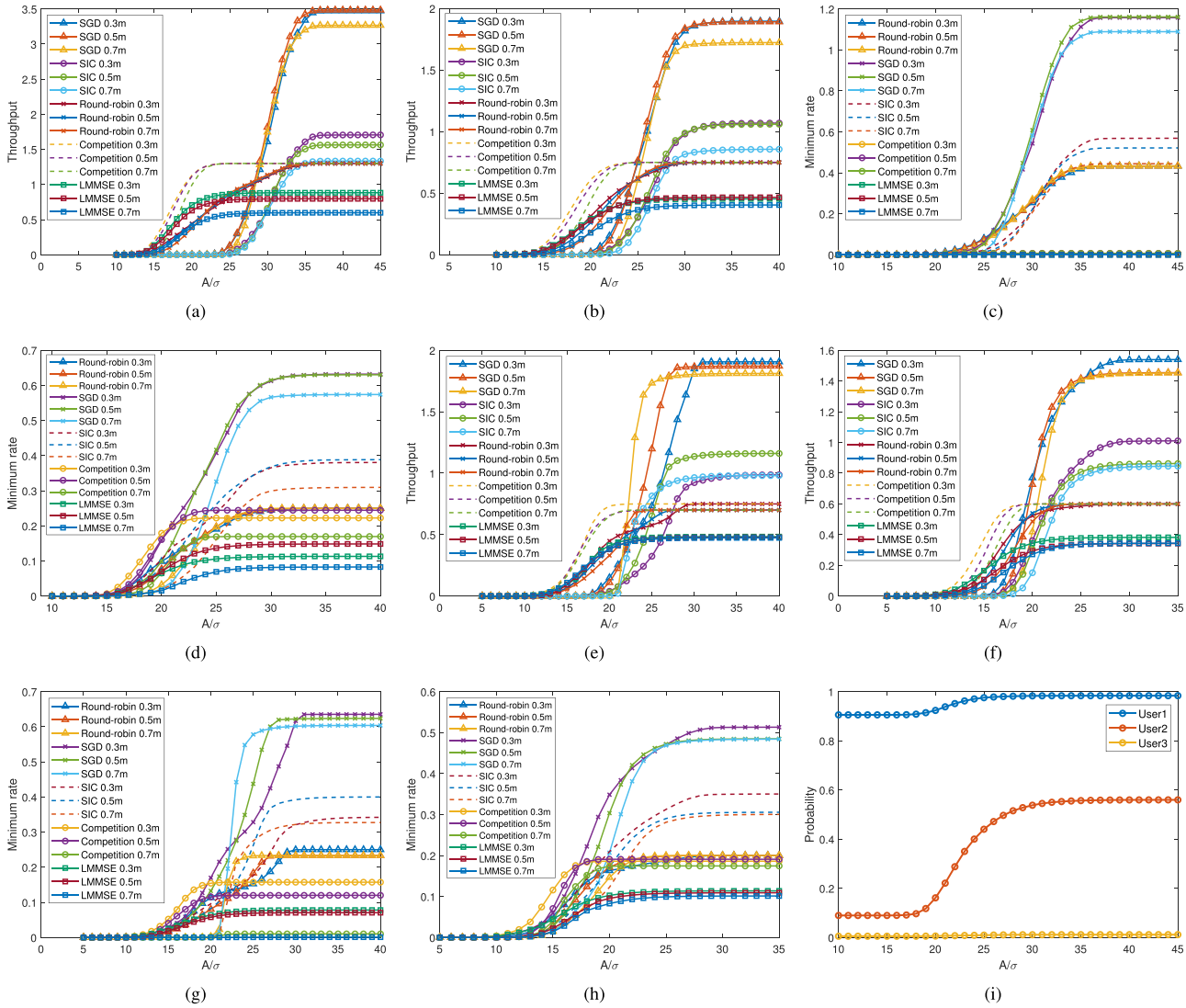

Fig. 13. Performance in deep wave pool experiments under fixed-rate mode. (a) Throughput, vertical, fixed container. (b) Throughput, parallel, fixed container. (c) Minimum rate, vertical, fixed container. (d) Minimum rate, parallel, fixed container. (e) Throughput, vertical, anchored container. (f) Throughput, parallel, anchored container. (g) Minimum rate, vertical, anchored container. (h) Minimum rate, parallel, anchored container. (i) Users' distribution in stage1.

TABLE II
AVERAGE LINK GAIN IN DEEP WATER POOL FOR FIXED USERS

	Direction	Left	Middle	Right
Depth=0.3 m	Parallel	0.1063	0.1174	0.1062
	Vertical	0.1071	0.3519	0.0351
Depth=0.5 m	Parallel	0.0866	0.1062	0.1036
	Vertical	0.1104	0.3331	0.0333
Depth=0.7 m	Parallel	0.0618	0.0900	0.0875
	Vertical	0.1120	0.2631	0.0321

TABLE III
AVERAGE LINK GAIN IN DEEP WATER POOL FOR ANCHORED USERS

	Direction	Left	Middle	Right
Depth=0.3 m	Parallel	0.1147	0.1160	0.1069
	Vertical	0.1265	0.1984	0.1342
Depth=0.5 m	Parallel	0.0959	0.0984	0.1002
	Vertical	0.1438	0.1807	0.1039
Depth=0.7 m	Parallel	0.0803	0.0796	0.0768
	Vertical	0.1456	0.1866	0.1130

Fig. 12(a) tends to move right, which means higher probability of larger-value link gain. Then, in parallel case, instantaneous different wave height for each user reduce such difference. Also, in the fourth and sixth row in Table II, the users in parallel situation have similar mean value of link gain. Then, in Fig. 12(b) and (c), the curves of each user have similar shape and a certain degree of overlap. Finally, due to broken waves, different PDFs exist in both sides of the middle node in the vertical case and

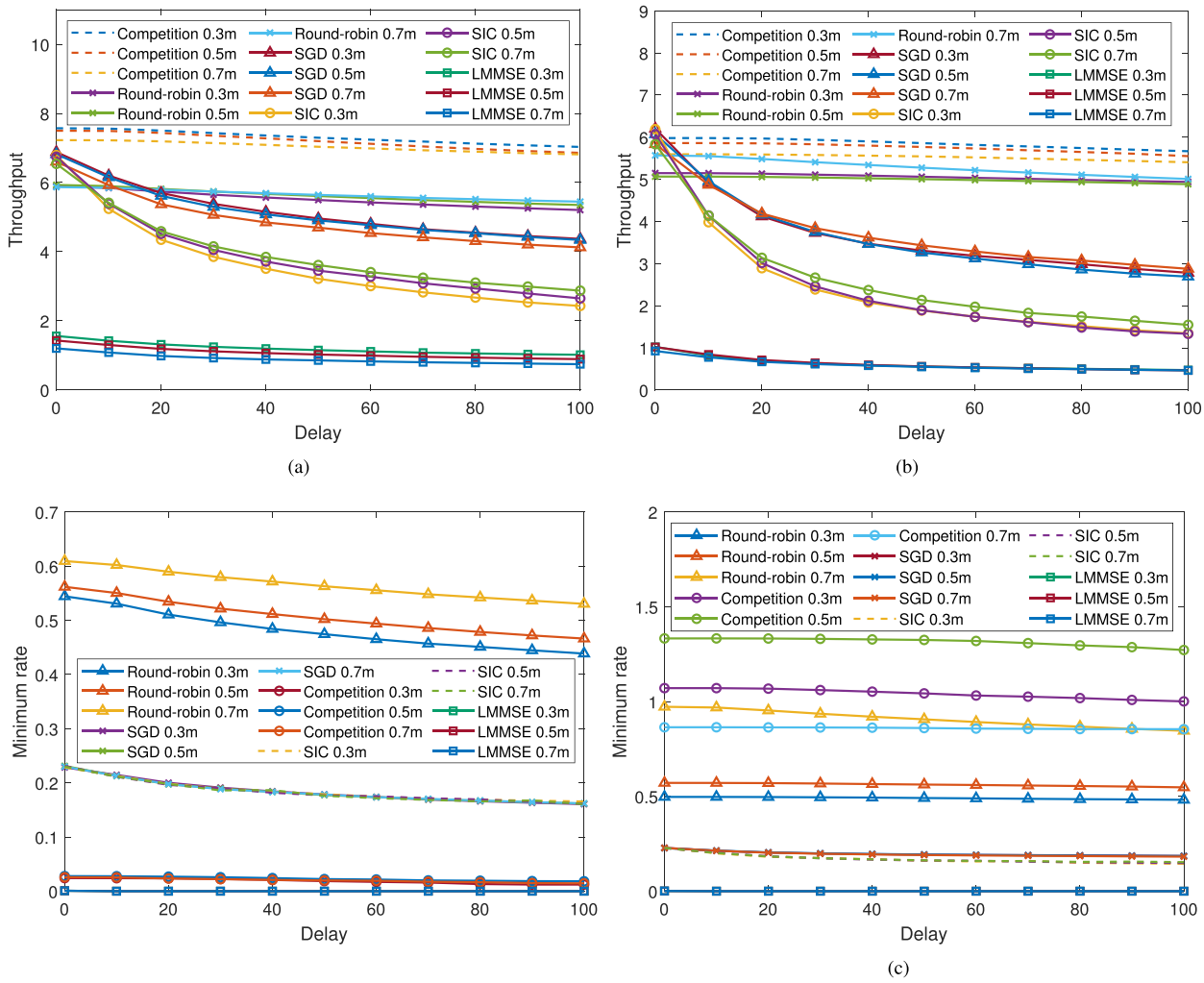

Fig. 14. Performance in deep wave pool experiments under allocated-rate mode with delay. (a) Throughput, vertical. (b) Throughput, parallel. (c) Minimum rate, vertical. (d) Minimum rate, parallel.

all users in the parallel case, as shown in Fig. 12. For example, the left and right users are not symmetric in vertical case due to broken wave, as shown in Table II. When the transmitters are anchored in the water current, the shaking decreases the average link gain difference among the transmitters when they are vertical to the wave direction. In parallel situation, the link gains maintain the same trend as that in the fixed-container situation, as shown in Table III.

A. Fixed Rate for Each User

Fig. 13 shows the throughput under different scheduling scheme changing against different PNR. In order to achieve the same outage probability, we allocate $R = 2.5$ bit/s/Hz to vertical situation and $R = 1.25$ bit/s/Hz to parallel situation because of different relative positions.

From Fig. 13, it is seen that under low PNR, the competition scheme shows lower outage probability and higher throughput. However, under high PNR, each decoding stage in SGD can ensure an acceptable probability to be successfully decoded, such that SGD shows the highest throughput. For minimum rate results, which have the same trend with the results in throughput, SGD shows better performance in Fig. 13(c) and (d) due to lower outage probability in fixed-rate mode. In case of anchored containers under water current, the SGD achieves the highest throughput and minimum rate under high PNR. However, comparing Fig. 13(a) and (e), the highest throughput is lower than that of fixed users due to the tilted light spot caused by current waves.

Due to interference cancellation, users in later decoding are unlikely to suffer outage under sufficiently high PNR. As shown in Fig. 13(i), earlier decoding stages consist of users with higher link gain with dominant outage under high PNR. This is the reason of allocating lower rate in parallel situation compared with that in vertical one.

B. Rate Allocation for Each User

Consider the scenario where the receiver utilizes CSI for rate allocation. As shown in Fig. 14, without delay, the optimal SGD achieves the highest throughput. Taking delay into account, we took 10 ms as a step size and plot the system throughput under

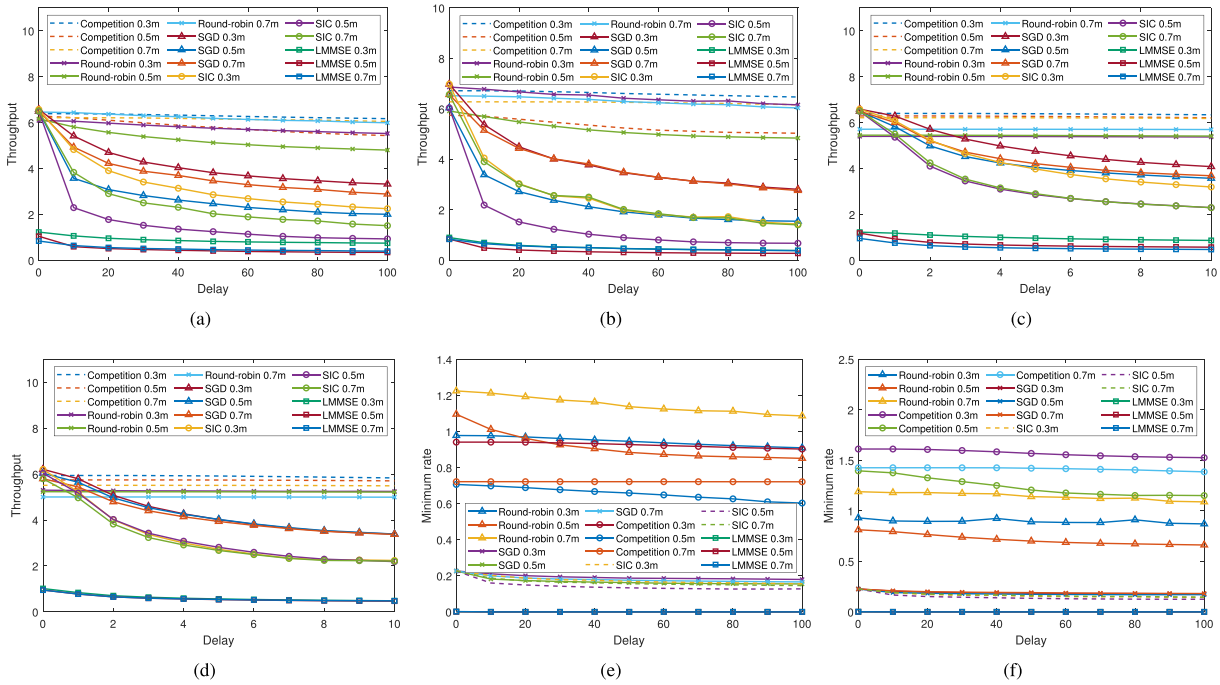

Fig. 15. Performance in deep wave pool experiments under allocated-rate mode with delay and anchored users. (a) Throughput, vertical. (b) Throughput, parallel. (c) Enlarged figure for delay less than 10 ms, vertical. (d) Enlarged figure for delay less than 10 ms, parallel. (e) Minimum rate, vertical. (f) Minimum rate, parallel.

delay between 0–100 ms. The result in deep wave pool is shown in Fig. 14.

It is seen that larger delay leads to lower throughput, while competition and round-robin lead to higher throughput compared to optimal SGD under delay longer than 10 ms. It is much easier to maintain reliable communication for a single user than multi-user access under channel fluctuation. Comparing Figs. 14 and 6(e), the critical delay where optimal SGD and competition have the same throughput in lab is longer than that in research center. This is because mixed large-scale and small-scale wave in research center increases the fluctuation of W2A-VLC channel.

Fig. 14(a) and (b) show the throughput of rate-allocation via the same optimization processing with the above. Compared with the results before optimization, the throughput of each scheme is significantly higher under delay due to lower outage probability. Obviously, the competition still shows the highest throughput due to its greedy user selection. Finally, as the same reason with fixed-rate case, vertical situation shows higher throughput than the parallel one.

In vertical case, round-robin holds the highest lower bound under different delay, as shown in Fig. 14(c). Comparing with SGD, SIC and LMMSE, round-robin ensures no interference among users and the outage for each user will not propagate to others. Due to equal access opportunity for each user, round-robin provide higher throughput to the user with lower link gain. In parallel case, round-robin and competition both maintain higher minimum rate with similar reason, as shown in Fig. 14(d). However, under 0.3m-depth and 0.5m-depth, the competition has a higher minimum rate than round-robin while round-robin shows higher throughput under 0.7m-depth. This is because the users tend to have similar average link gain in parallel case, which leads to similar access opportunity even using competition scheme, as shown in Table II.

Due to lower middle user link gain in anchored-container situation, the competition access scheme demonstrates a smaller gap with round-robin in Fig. 15(a) than that in Fig. 14(a). However, the minimum rate of round-robin scheme is higher than that of competition scheme in vertical situation. When the transmitters are parallel to the wave direction, the throughput and minimum rate of the competition scheme is higher than that of round-robin scheme. Moreover, as shown in enlarged details in Fig. 15(c) and (d), the throughputs of SGD and round-robin intersect at about 2 ms, which is shorter than the intersections in Fig. 14(a) and (b). Such results imply that a quicker feedback is needed for the SGD.

VI. Conclusion

We have established a multi-user W2A-VLC system in deep wave pool under wavy water conditions. Based on simulation and experimental results, we have extracted link gain when the user line is parallel or vertical to the wave direction. It is observed that the statistic characteristics of link gain from each user tends to be different in parallel case while it tends to overlap with each other in vertical case. To make the analysis more realistic, delay caused by transmission and data processing has been taken into account. We have adopted several scheduling schemes under different rate modes and compared their performance from the perspective of average system throughput and fairness. The results show that the optimal SGD provide the highest throughput and minimum rate in fixed-rate mode. Besides, competition scheduling has the best throughput performance in delay-based allocated-rate mode, but it maintains the highest minimum rate

only in parallel case while round robin scheduling performs more fairly in vertical case.

REFERENCES

[1] Z. Zeng, S. Fu, H. Zhang, Y. Dong, and J. Cheng, "A survey of underwater optical wireless communications," *IEEE Commun. Surv. Tuts.*, vol. 19, no. 1, pp. 204–238, Firstquarter 2017.

[2] H. Luo, J. Wang, F. Bu, R. Ruby, K. Wu, and Z. Guo, "Recent progress of air/water cross-boundary communications for underwater sensor networks: A review," *IEEE Sensors J.*, vol. 22, no. 9, pp. 8360–8382, May 2022.

[3] L.-K. Chen, Y. Shao, and Y. Di, "Underwater and water-air optical wireless communication," *J. Lightw. Technol.*, vol. 40, no. 5, pp. 1440–1452, Mar. 2022.

[4] Z. Xu, W. Liu, Z. Wang, and L. Hanzo, "Petahertz communication: Harmonizing optical spectra for wireless communications," *Digit. Commun. Netw.*, vol. 7, no. 4, pp. 605–614, Nov. 2021.

[5] X. Sun et al., "Field demonstrations of wide-beam optical communications through water–air interface," *IEEE Access*, vol. 8, pp. 160480–160489, 2020.

[6] N. Huang, C. Gong, C. Fu, T. Wei, and Z. Xu, "Preliminary investigation of air-to-water visible light communication link under strong ambient light," in *Proc. IEEE 94th Veh. Technol. Conf.*, 2021, pp. 1–5.

[7] Z. Rahman, S. M. Zafaruddin, and V. K. Chaubey, "Direct air-to-underwater optical wireless communication: Statistical characterization and outage performance," *IEEE Trans. Veh. Technol.*, vol. 72, no. 2, pp. 2655–2660, Feb. 2023.

[8] M. Rauf, M. Aamir, and A. M. Khan, "A prospect of efficient radio-frequency based underwater wireless data transfer," in *Proc. IEEE Glob. Conf. Wireless Opt. Technol.*, 2020, pp. 1–5.

[9] E. M. Sozer, M. Stojanovic, and J. G. Proakis, "Underwater acoustic networks," *IEEE J. Ocean. Eng.*, vol. 25, no. 1, pp. 72–83, Jan. 2000.

[10] F. Tonolini and F. Adib, "Networking across boundaries: Enabling wireless communication through the water-air interface," in *Proc. ACM Special Int. Group Data Commun.*, 2018, pp. 117–131.

[11] F. Qu et al., "Cross-medium communication combining acoustic wave and millimeter wave: Theoretical channel model and experiments," *IEEE J. Ocean. Eng.*, vol. 47, no. 2, pp. 483–492, Apr. 2022.

[12] Y. Gai et al., "A cross-medium uplink communication model merging acoustic and millimeter waves," *J. Mar. Sci. Eng.*, vol. 11, no. 11, Nov. 2023, Art. no. 2102.

[13] P. A. Hoeher, J. Sticklus, and A. Harlakin, "Underwater optical wireless communications in swarm robotics: A tutorial," *IEEE Commun. Surv. Tuts.*, vol. 23, no. 4, pp. 2630–2659, Fourthquarter 2021.

[14] Z. Wei et al., "2 Gbps/3 m air–underwater optical wireless communication based on a single-layer quantum dot blue micro-LED," *Opt. Lett.*, vol. 45, no. 9, pp. 2616–2619, May 2020.

[15] P. Nabavi, A. S. Haq, and M. Yuksel, "Empirical modeling and analysis of water-to-air optical wireless communication channels," in *Proc. IEEE Int. Conf. Commun. Workshops*, 2019, pp. 1–6.

[16] T. Lin, C. Gong, J. Luo, and Z. Xu, "Dynamic optical wireless communication channel characterization through air-water interface," in *Proc. IEEE/CIC Int. Conf. Commun. China*, 2020, pp. 173–178.

[17] T. Lin, N. Huang, C. Gong, J. Luo, and Z. Xu, "Preliminary characterization of coverage for water-to-air visible light communication through wavy water surface," *IEEE Photon. J.*, vol. 13, no. 1, pp. 1–13, Feb. 2021.

[18] C. Fu et al., "Anti error and erasure coding for water-to-air visible light communication through wavy water surface with wave height up to 0.6 meters," *Opt. Exp.*, vol. 30, no. 11, pp. 18743–18761, May 2022.

[19] T. Lin et al., "Waving effect characterization for water-to-air optical wireless communication," *IEEE J. Lightw. Technol.*, vol. 41, no. 1, pp. 120–136, Jan. 2023.

[20] Y. Di, Y. Shao, and L.-K. Chen, "Real-time wave mitigation for water-air OWC systems via beam tracking," *IEEE Photon. Technol. Lett.*, vol. 34, no. 1, pp. 47–50, Jan. 2022.

[21] Y. Shao, R. Deng, J. He, K. Wu, and L.-K. Chen, "Real-time 2.2-Gb/s water-air OFDM-OWC system with low-complexity transmitter-side DSP," *IEEE J. Lightw. Technol.*, vol. 38, no. 20, pp. 5668–5675, Oct. 2020.

[22] T. Li, Y. Yang, X. Gao, H. Zhang, and T. Lian, "Laser transmission model for a cross-medium uplink channel," in *Proc. IEEE 9th Joint Int. Inf. Technol. Artif. Intell. Conf.*, 2020, vol. 9, pp. 454–459.

[23] M. S. Islam, M. Younis, and A. Ahmed, "Communication through air water interface using multiple light sources," in *Proc. IEEE Int. Conf. Commun.*, 2018, pp. 1–6.

[24] S. Li and L. Yang, "Analysis of a mixed multi-user underwater acoustic communication/free space optical heterogeneous relaying system," *IEEE Internet Things J.*, vol. 11, no. 11, pp. 20718–20730, Jun. 2024.

[25] X. Bao, X. Zhu, T. Song, and Y. Ou, "Protocol design and capacity analysis in hybrid network of visible light communication and OFDMA systems," *IEEE Trans. Veh. Technol.*, vol. 63, no. 4, pp. 1770–1778, May 2014.

[26] H. Yang, C. Chen, W.-D. Zhong, and A. Alphones, "Joint precoder and equalizer design for multi-user multi-cell MIMO VLC systems," *IEEE Trans. Veh. Technol.*, vol. 67, no. 12, pp. 11354–11364, Dec. 2018.

[27] H. Wang, Z. Zhang, B. Zhu, J. Dang, L. Wu, and Z. Gong, "Space division multiple access based on OIRS in multi-user FSO system," *IEEE Trans. Veh. Technol.*, vol. 71, no. 12, pp. 13403–13408, Dec. 2022.

[28] Y. Le, L. Ma, W. Cheng, X. Cheng, and B. Chen, "A time fairness-based MAC algorithm for throughput maximization in 802.11 networks," *IEEE Trans. Comput.*, vol. 64, no. 1, pp. 19–31, Jan. 2015.

[29] S. Bi and Y. J. A. Zhang, "Outage-optimal TDMA based scheduling in relay-assisted MIMO cellular networks," *IEEE Trans. Wireless Commun.*, vol. 11, no. 4, pp. 1488–1499, Apr. 2012.

[30] F. Kelly, "Charging and rate control for elastic traffic," *Eur. Trans. Telecommun.*, vol. 8, no. 1, pp. 33–37, Jan. 1997.

[31] L. Li, M. Pal, and Y. R. Yang, "Proportional fairness in multi-rate wireless LANs," in *Proc. IEEE 27th Conf. Comput. Commun.*, 2008, pp. 1004–1012.

[32] S. Huaizhou, R. V. Prasad, E. Onur, and I. G. M. M. Niemegeers, "Fairness in wireless networks: Issues, measures and challenges," *IEEE Commun. Surv. Tuts.*, vol. 16, no. 1, pp. 5–24, Firstquarter 2014.

[33] A. Chaaban, J.-M. Morvan, and M.-S. Alouini, "Free-space optical communications: Capacity bounds, approximations, and a new sphere-packing perspective," *IEEE Trans. Commun.*, vol. 64, no. 3, pp. 1176–1191, Mar. 2016.

[34] G. Zheng, C. Gong, and Z. Xu, "Constrained partial group decoding with max–min fairness for multi-color multi-user visible light communication," *IEEE Trans. Commun.*, vol. 67, no. 12, pp. 8573–8584, Dec. 2019.

[35] D. Tse and P. Viswanath, *Fundamentals of Wireless Communication*. New York, NY, USA: Cambridge Univ. Press, 2005.

[36] H. Wang et al., "Performance analysis of multi-branch reconfigurable intelligent surfaces-assisted optical wireless communication system in environment with obstacles," *IEEE Trans. Veh. Technol.*, vol. 70, no. 10, pp. 9986–10001, Oct. 2021.

[37] J. Wei, C. Gong, N. Huang, and Z. Xu, "Channel modeling and signal processing for array-based visible light communication system under link misalignment," *IEEE Photon. J.*, vol. 14, no. 2, pp. 1–10, Apr. 2022.

[38] V. K. Lau and W. K. Ng, "Per-user packet outage analysis in slow multiaccess fading channels with successive interference cancellation for equal rate applications," *IEEE Trans. Wireless Commun.*, vol. 7, no. 5, pp. 1754–1763, May 2008.

[39] N. Prasad and X. Wang, "Outage minimization and rate allocation for the multiuser Gaussian interference channels with successive group decoding," *IEEE Trans. Inf. Theory*, vol. 55, no. 12, pp. 5540–5557, Dec. 2009.

[40] C. Gong, A. Tajer, and X. Wang, "Interference channel with constrained partial group decoding," *IEEE Trans. Commun.*, vol. 59, no. 11, pp. 3059–3071, Nov. 2011.

Tianjian Wei received the B.S. degree from Northwestern Polytechnical University, Xi'an, China, in 2021. He is currently working toward the Ph.D. degree with the University of Science and Technology of China, Hefei, China. His research interests include water to air visible light communication and multiuser scheduling.

Tianrui Lin received the B.S. degree from the University of Electronic Science and Technology of China, Chengdu, China, in 2019. He is currently working toward the Ph.D. degree with the Optical Wireless Communication, University of Science and Technology of China, Hefei, China. His research interests include water to air visible light communication and MIMO communication.

Nuo Huang received the B.S. degree in electronics and information engineering from the Huazhong University of Science and Technology, Wuhan, China, in 2012, and the Ph.D. degree in information and communication engineering from the National Mobile Communications Research Laboratory, Southeast University, Nanjing, China, in 2019. From 2015 to 2017, he was a Visiting Student with the Department of Electrical Engineering, Columbia University, New York, NY, USA. He is currently an Associate Professor with the Department of Electronic Engineering and Information Science, University of Science and Technology of China, Hefei, China. He was selected by the National Postdoctoral Program for Innovative Talents in 2019. His research interests include resource allocation and transceiver design in wireless (optical) communications.

Chunfang Fu received the B.S. degree from the Dalian University of Technology, Dalian, China, in 2020, and the M.S. degree from the University of Science and Technology of China, Hefei, China, in 2023. His research interests include water to air visible light communication and channel coding.

Xinhui Liu received the B.S. degree in mechanical and electronic engineering from Qingdao University, Qingdao, China, in 2004, and the M.S. degree in mechanical design and theory from the Nanjing University of Aeronautics and Astronautics, Nanjing, China, in 2007. He is currently a Senior Engineer with China Ship Scientific Research Center, Wuxi, China. His research focuses on design of underwater structures.

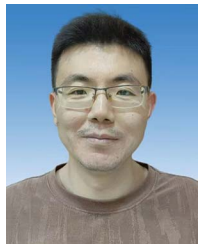

Liang Su received the B.S. degree from Zhejiang Ocean University, Zhoushan, China, in 2010, and the M.S. degree in China Ship Scientific Research Center, Wuxi, China, in 2013. His research interests include theoretical analysis and experimental study of multiphase flow.

Li Tang received the B.S. degree from Jiangnan University, Wuxi, China, in 2012, and the M.S. degree in control engineering from Peking University, Beijing, China, in 2015. He is currently a Senior Engineer with China Ship Science Research Center, Wuxi. His research interests include measurement and control technology, nonlinear control system, and control modeling and simulation.

Qingqing Hu received the B.S. degree from the Dalian University of Technology, Dalian, China, in 2016, and the M.S. degree in 2019, from the University of Science and Technology of China, Hefei, China, where she is currently working toward the Ph.D. degree. Her research interests include information security, signal processing, and visible light communication.

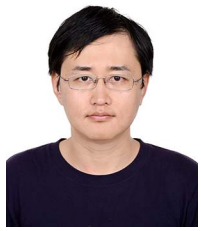

Chen Gong (Senior Member, IEEE) received the B.S. degree in electrical engineering and mathematics (minor) from Shanghai Jiaotong University, Shanghai, China, in 2005, the M.S. degree in electrical engineering from Tsinghua University, Beijing, China, in 2008, and the Ph.D. degree from Columbia University, New York, NY, USA, in 2012. He was a Senior Systems Engineer with the Qualcomm Research, San Diego, CA, USA, from 2012 to 2013. He is currently a Faculty Member with the University of Science and Technology of China, Hefei, China. His research interests include wireless communications, optical wireless communications, and signal processing. He was the recipient of the Hong Kong Qiushi Outstanding Young Researcher Award in 2016.